国立大学法人 九州工業大学

2023 年 10 月 11 日

振幅・位相ノイズによる確率共鳴-逆確率共鳴の転移現象の制御

本学大学院情報工学研究院物理情報研究系の許宗君教授が研究代表者を務める非平衡散逸系の研究グループは、ノイズのポジティブ効果として知られている確率共鳴現象*1 を液晶の電気対流系*2 を用いて調査しました。数値計算と実験調査から確率共鳴現象及び逆確率共鳴現象を自由に発生させたり両共鳴現象を転移させたりする手法を発見しました。この手法は適切にカラー化した振幅と位相ノイズを絶妙に配合する方式で、バイオテクノロジー、画像処理技術、センサー工学などの多くの関連分野に応用が期待されます。

ポイント

- **確率共鳴と逆確率共鳴を発生させ、両共鳴現象の転移を制御する**
- **カラーノイズ*3 の効果を実証する**
- **振幅ノイズと位相ノイズの絶妙な配合がカギとなる**

通常、ノイズといえば不要な信号であり、その発生原因と除去方法の研究が求められます。電子機器などの誤作動をなくしたい、ノイズのない快適な環境で暮らしたいというのが我ら人間の願いであるからです。しかし、ノイズはそのネガティブなイメージばかりではありません。例えば、1/*f* ノイズは扇風機の風を自然の風のゆらぎに近い風へと変えるところに応用されています。また、普通は検知できない微弱な信号に適切なノイズを加えることによって、その微弱信号を検出する確率共鳴手法は広く知られています。

これまで物理、生物、情報、脳科学などの分野で確率共鳴現象（Stochastic Resonance, SR）と逆確率共鳴現象（Inverse Stochastic Resonance, ISR）が発見され応用分野も多岐にわたっています。しかしながら、一つのシステムで SR と ISR を自由に発生させたり、両共鳴現象を転移させたりすることはできませんでした。その理由は通常の振幅型ホワイトノイズのみを使用していたからです。そこで、本研究では、

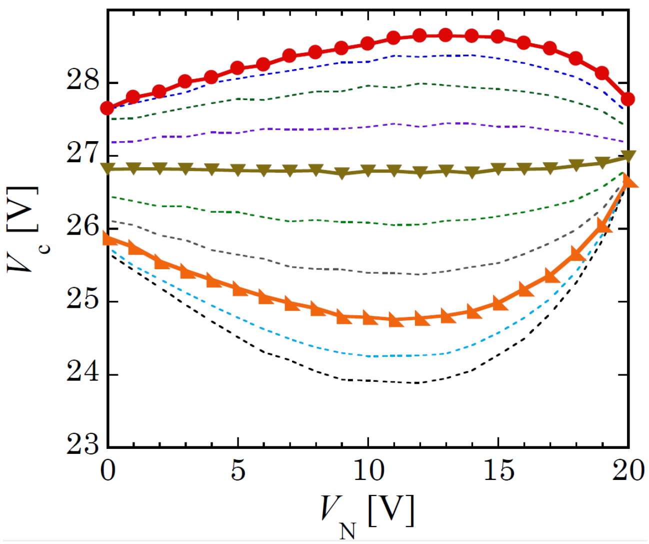

(a)

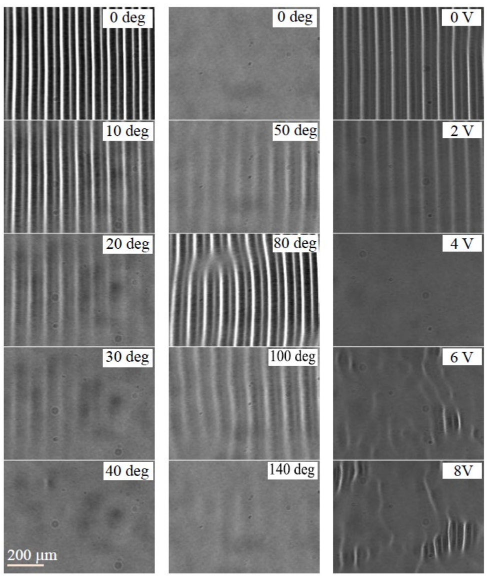

(b1) (b2) (b3)

振幅と位相の両ノイズをカラー化し適切に配合する手法を用いて、SR と ISR の調査を行いました。調査で用いた液晶の電気対流現象はある電圧（V_c）以上で対流が発生します。その交流電界に振幅と位相ノイズを乗せると、V_c は大きくなったり小さくなったりします。

図(a)は振幅ノイズ強度 V_N を変えながら V_c の変化を示したグラフであり、その実験曲線は上から順番に位相ノイズ強度ϕ_N を強めながら測定した結果です。最大値を示すカーブが ISR に相当する振る舞いであり、図(b3)が対応する電気対流の様子を表しています。すなわち、ある電圧条件に発生した電気対流（図中の縞模様）は、振幅ノイズ強度 V_N を上げると消えたり、さらに上げると再び現れたりする、不思議な現象が実験で確認できます。さらに、図(b2)は位相ノイズ強度ϕ_N を上げると電気対流が現れるが、さらに上げると消えるという SR を示しています。これら SR と ISR を起こすノイズは、位相ノイズ強度ϕ_N を上げると電気対流が徐々に消えていく図(b1)に示すような直感的なノイズのイメージと全く異なります。さらに、図(a)は、最大値を示すカーブ ISR から最小値を示すカーブ SR への転移も示しています。これは SR と ISR の研究において世界で初めて示された成果であり、今後、関連する様々な分野においても応用が期待されます。

このような発見に至った研究手法においてカギとなるのは、振幅・位相ノイズを適切にカラー化し配合することです。本研究では、その配合によって、図(a)以外にも様々な閾値電圧 V_c の振る舞いについて数値計算を用いて明らかにしました。

なお、この研究成果は、2023 年 10 月 7 日（土）午前 1 時（日本時間）に英国の科学オープンアクセス誌「Scientific Reports (Springer Nature 社)」に掲載されました。

*1 確率共鳴現象：	非線形システムにおいて、外部の確率的なノイズが存在する条件下で、システムの性能や感度が最適になる現象を指します。具体的には、確率的なノイズがシステムに追加されると、システムの出力が増幅され、信号検出や情報伝達などのタスクに対する性能が向上することがあります。
*2 電気対流系：	液晶層内の電場が十分に強い場合、クーロン力が液晶の粘弾性力に打ち勝ち系内に不安定性が引き起こされ、異方性流体（液晶）の運動が誘発される現象を示すシステムです。
*3 カラーノイズ（Colored noise）：	通常のホワイトノイズは、全ての周波数成分が均等に分布しているランダムな信号であるのに対し、カラーノイズは特定の周波数帯域でエネルギーが強化または減衰されたノイズを指します。本研究では Low-Pass Filter で制御したカラーノイズを使用しています。

【論文の詳細情報】

タイトル：	Control of stochastic and inverse stochastic resonances in a liquid-crystal electroconvection system using amplitude and phase noises
著 者 名：	Jong-Hoon Huh, Masato Shiomi, Naoto Miyagawa
雑　　誌：	Scientific Reports (Springer Nature 社)
DO I　　：	https://doi.org/10.1038/s41598-023-44043-4

※本研究は JSPS 科研費 JP18K03464, JP22K03470 の助成を受けたものです。

【研究内容に関するお問い合わせ】
九州工業大学 大学院情報工学研究院 物理情報研究系教授 許宗君
電話：0948-29-7897　Mail：huh@phys.kyutech.ac.jp

【報道に関するお問い合わせ】
九州工業大学総務課広報係
電話：093-884-3007　Mail：pr-kouhou@jimu.kyutech.ac.jp

scientific reports

OPEN

Control of stochastic and inverse stochastic resonances in a liquid-crystal electroconvection system using amplitude and phase noises

Jong-Hoon Huh✉, Masato Shiomi & Naoto Miyagawa

Stochastic and inverse stochastic resonances are counterintuitive phenomena, where noise plays a pivotal role in the dynamics of various biological and engineering systems. Even though these resonances have been identified in various systems, a transition between them has never been observed before. The present study demonstrates the presence of both resonances in a liquid crystal electroconvection system using combined amplitude and phase noises, which correspond to colored noises with appropriate cutoff frequencies (i.e., finite correlation times). We established the emergence of both resonances and their transition through systematic control of the electroconvection threshold voltage using these two noise sources. Our numerical simulations were experimentally confirmed and revealed how the output performance of the system could be controlled by combining the intensity and cutoff frequency of the two noises. Furthermore, we suggested the crucial contribution of a usually overlooked additional phase noise to the advancements in various noise-related fields.

Stochastic resonance (SR) is an attractive counterintuitive phenomenon induced by noise combined with a deterministic signal[1], which enhances the output performance of unknown weak signals below the threshold of detection tools. Usually, SR shows a maximal output performance peak corresponding to the signal-to-noise ratio at a moderate optimal noise level. Since Benzi et al. first suggested this phenomenon and its underlying mechanism in a study on ice-age cycles[2,3], SR has been extensively investigated in various fields, including physics[4,5], chemistry[6,7], biology[8,9], information technology[10,11], and brain science[12,13]. By contrast, an opposing phenomenon known as the inverse SR (ISR) was initially discovered in a neural system[14–16], showing a minimal output performance peak at a moderate optimal noise intensity. Later, ISR was also reported in other systems such as ecological systems and during electroconvection (EC)[17,18].

The mechanisms of both SR[1] and ISR[19] are generally described using an expanded Langevin equation as follows:

$$\frac{dx}{dt} = -\frac{\partial[\phi(x) - A_0 x \cos \Omega t]}{\partial x} + \zeta(t). \tag{1}$$

In standard SR, the presence of a weak deterministic signal (i.e., $A_0 \neq 0$) and noise $\zeta(t)$ dictates that the potential function $\phi(x)$ for the system of interest must be bistable (i.e., two stable minima)[1]. Conversely, ISR can be obtained in the absence of a weak deterministic signal (i.e., $A_0 = 0$) if the two minima have different depths and widths. Consequently, the reflection symmetry ($x \rightarrow -x$) in the quartic double-well potential is broken for ISR[19], whereas the deterministic signal ($A_0 \neq 0$) breaks the symmetry in SR. In other words, the symmetry-broken potential is periodic ($\Omega \neq 0$) for SR and stationary ($\Omega = 0$) for ISR[19]. In contrast to the standard SR introduced by Benzi et al., Sutera suggested a pure noise-induced transition ($A_0 = 0$) to explain the ice-age cycles[20]. Interestingly, nonstandard SR was also observed[19] in the absence of a signal ($A_0 = 0$), which is often referred to as coherent resonance[1]. Breaking the reflection symmetry of the two-minimum potential is essential to generate standard

Department of Physics and Information Technology, Faculty of Computer Science and Systems Engineering, Kyushu Institute of Technology, Fukuoka 820-8502, Japan. ✉email: huh@phys.kyutech.ac.jp

SR and ISR. Moreover, the noise $\zeta(t)$ in Eq. (1) is *additive*, i.e., independent of the variable x[21,22]. Similarly, *multiplicative* noise $\xi(t)$ [i.e., $x\xi(t)$] can provide SR[22–24] and ISR[17].

To the best of our knowledge, SR and ISR have never been observed concurrently in any actual system. To expand the use of SR and ISR into advanced applications, it is necessary to control both resonances and provide a transition between them, enabling the subsequent control of both desired and undesired system performances according to actual needs. In our previous studies, we confirmed the presence of both SR[25] and ISR[17] independently in a nonequilibrium system using different noises, i.e., *phase* noise for SR and *amplitude* noise for ISR. In the present study, we appropriately combined these two types of noise in order to control both resonances and the transition between them. In addition to the commonly used amplitude noise, our method utilized the usually overlooked phase noise[25,26]. Moreover, we used a *colored* noise with a finite autocorrelation time ($\tau_c \neq 0$)[17,21,22,27–31], instead of the conventional quasi-white noise ($\tau_c \approx 0$)[2–13,27].

In this report we demonstrate the transition between SR and ISR via a smooth variation of the output performance using ac-driven electroconvection in a nematic liquid crystal (NLC)[32–36]. Our findings show how to control monotonic and nonmonotonic variations of the EC threshold using colored amplitude and phase noises. The unusual nonmonotonic behavior of the threshold confirms the presence of both SR and ISR, providing maximal and minimal peaks of the EC pattern performance by efficiently facilitating and suppressing EC around a moderate optimal level of the amplitude and phase noises.

In this numerical study, the threshold voltage V_c of the EC was calculated using the one-dimensional Carr – Helfrich equations as follows[32–35]:

$$\dot{q} + \frac{q}{\tau} + \sigma_{\mathrm{H}} \frac{V(t)}{d} \psi = 0, \tag{2}$$

$$\dot{\psi} + \lambda \left[E_0^2 + \left(\frac{V(t)}{d} \right)^2 \right] \psi + \frac{q}{\eta} \frac{V(t)}{d} = 0. \tag{3}$$

Here, $q(t)$ and $\psi(t)$ represent the space-charge density and curvature ($\psi = \partial\varphi/\partial x$) of the director for the deviation angle φ from the initial director $\boldsymbol{n}_0$ $(//\hat{\boldsymbol{x}})$ at $V = 0$, respectively (Fig. 1a), and $\boldsymbol{n}$ corresponds to a unit vector indicating a locally averaged direction of the rod-like molecules of NLCs. The values of τ, σ_{H}, λ, $E_0{}^2$, and η are determined by material parameters such as the electric and viscoelastic properties of the NLC with a thickness

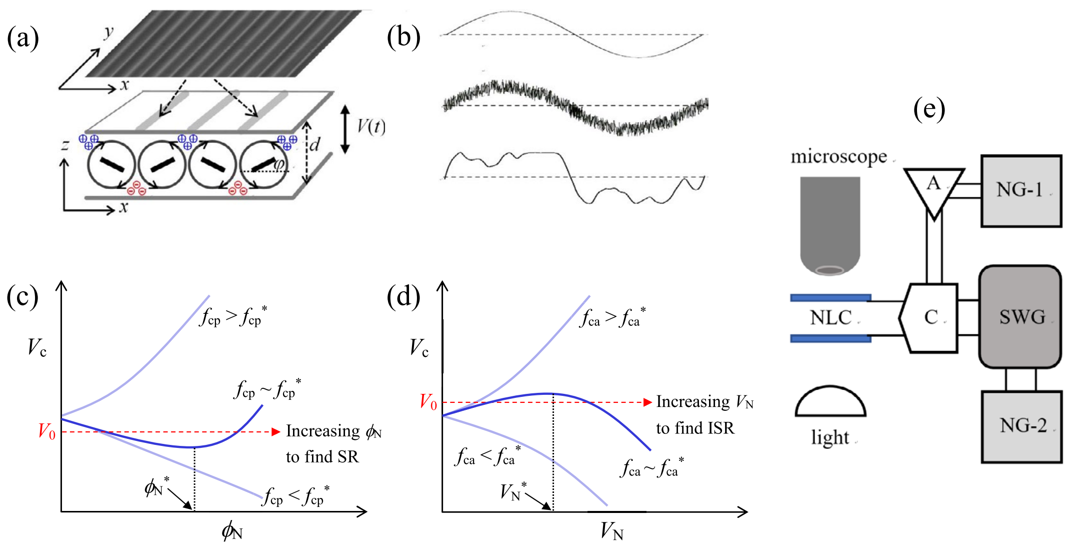

Figure 1. Colored noises-induced threshold variation of ac-driven electroconvection (EC). (**a**) A schematic representation of EC driven by Coulomb forces on electric charges (blue circle with plus sign, red circle with minus sign) in a nematic liquid crystal (NLC). The rods in the vortices of EC indicate the director $\boldsymbol{n}$ of the NLC. Above a threshold V_c, EC is observed as a roll pattern (i.e., Williams domain) in the *xy* plane, which results from the periodic director angle $\varphi(x)$. (**b**) Original sinusoidal voltage $V(t)$ (i.e., $\phi_N = V_N = 0$) (top) and voltages superposed by amplitude noise (i.e., $\phi_N = 0$, $V_N \neq 0$) (middle) and phase noise (i.e., $\phi_N \neq 0$, $V_N = 0$) (bottom). (**c**) Threshold voltage V_c as a function of phase-noise intensity ϕ_N. (**d**) Threshold voltage V_c as a function of amplitude-noise intensity V_N. (**e**) Experimental system for EC under two noise sources (*NG-1* noise generator for amplitude noise, *NG-2* noise generator for phase noise, *SWG* sinusoidal wave generator, *A* amplifier, *C* combiner). The functions of $V_c(\phi_N)$ and $V_c(V_N)$ highly depend on the cutoff frequency f_c of the colored noise. In (**c**), nonmonotonic $V_c(\phi_N)$ is observed for $f_{cp} \sim f_{cp}^*$ of phase noise, indicating stochastic resonance (SR). In (**d**), reversed nonmonotonic $V_c(V_N)$ is observed for $f_{ca} \sim f_{ca}^*$ of amplitude noise, indicating inverse stochastic resonance (ISR). See Refs[17,25]. for our previous results [$V_c(V_N)$ and $V_c(\phi_N)$] and corresponding EC pattern changes.

d. To examine the behavior of V_c in the presence of noise, we used an electric voltage $V(t)$ with amplitude and phase noises, as shown in Eq. (4):

$$V(t) = \sqrt{2}V\cos\left[2\pi f_0 t + \phi_N \xi_p(t)\right] + A_N \xi_a(t). \tag{4}$$

Here, $\xi_p(t)$ and $\xi_a(t)$ correspond to phase and amplitude Gaussian-colored noises with cutoff frequencies $f_c = 1/(2\pi\tau_c)$, respectively, and ϕ_N and $V_N = \sqrt{<(A_N\xi_a(t))^2>}$ are the amplitude and phase noise intensities, respectively. Technically, f_c can be controlled by low pass filters[25,27]. Hereafter, f_{cp} and f_{ca} indicate the cutoff frequencies for the phase and amplitude noises, respectively. In the EC system, the two noises superimposed on an initial ac field (Fig. 1b) is multiplicative[17,22,24,37] because $V(t)$ is directly coupled with the angle φ [in Fig. 1a for $\psi = \partial\varphi/\partial x$ in Eqs. (2) and (3)]. The EC arises from $\varphi = 0$ (for $V < V_c$) to $\varphi \neq 0$ (for $V > V_c$). Here, the additive noise $\zeta(t)$ in Eq. (1), corresponding to the thermal fluctuations in the NLC, can be neglected because it affects considerably less EC than the multiplicative noise[36,38].

To better understand the present results, the V_c variations obtained using a single noise intensity (i.e., ϕ_N or V_N) are schematically presented in Fig. 1c, d, as reported in our previous results[17,25]. Figure 1c shows that a colored phase noise with ϕ_N ($f_{cp} \sim f_{cp}^*$) at a fixed initial signal V_0 (with a fixed f_0) triggers the nonmonotonic behavior of $V_c(\phi_N)$, indicating SR[25]. The characteristic cutoff frequencies f_{cp}^* and f_{ca}^* are highly dependent on f_0 (e.g., $f_{cp}^* < 2f_0$ and $f_{ca}^* < 20f_0$ for a typical NLC; p-methoxybenzylidene-p'-n-butylaniline (MBBA) was used in this study), and their applicable frequency range is $f_c^* \pm \Delta f_c$ (e.g., $\Delta f_{cp} = \pm 0.5 f_{cp}^*$ and $\Delta f_{ca} = \pm 0.5 f_{ca}^*$ for MBBA). $V_c(\phi_N)$ demonstrates a minimal peak at ϕ_N^* that provides the maximal difference between V_0 and V_c (i.e., $\alpha = V_0 - V_c$) at ϕ_N^*. Thus, the maximal performance of the EC pattern is obtained at ϕ_N^*, resulting from a maximal angle φ (Fig. 1a). Accordingly, a rest state ($\varphi = 0$) held at $\phi_N = 0$ (i.e., $\alpha < 0$) changes into EC (i.e., $\alpha > 0$) when ϕ_N increases, which then disappears at high ϕ_N (i.e., $\alpha < 0$). Therefore, the performance (φ) of the EC patterns showed a typical *bell-shaped* type for SR[25]. Conversely, as shown in Fig. 1d, a colored amplitude noise V_N ($f_{ca} \sim f_{ca}^*$) provides a reversed nonmonotonic function $V_c(V_N)$ that indicates ISR[17]. Thus, EC ($\varphi \neq 0$) generated at $V_N = 0$ (i.e., $\alpha > 0$) disappears (i.e., $\varphi = 0$) around $V_N = V_N^*$ (i.e., $\alpha < 0$) and then reappears (i.e., $\varphi \neq 0$) at $V_N >> V_N^*$ (i.e., $\alpha > 0$). In contrast to noise with $f_{cp} \sim f_{cp}^*$ (and $f_{ca} \sim f_{ca}^*$), noise with $f_{cp} > f_{cp}^*$ (and $f_{ca} > f_{ca}^*$) induces a monotonic increase in $V_c(\phi_N)$ [and $V_c(V_N)$], whereas noise with $f_{cp} < f_{cp}^*$(and $f_{ca} < f_{ca}^*$) induces a monotonic decrease in $V_c(\phi_N)$ [and $V_c(V_N)$], as shown in Figs. 1c and 1d, respectively. In these cases, SR and ISR cannot be obtained. For extremely high f_c [i.e., white noise with $f_{cp} \to \infty$ (and $f_{ca} \to \infty$)], the occurrence of EC is suppressed by the completely random action of noises on the motion of q and ψ in Eqs. (2) and (3)[37,39]. Note that although SR and ISR can be found independently, they do not transit between each other.

Results

Numerical results for the EC threshold

The EC threshold (V_c) was examined in the presence of both noises. Figure 2 demonstrates the phase noise-induced behavior of $V_c(\phi_N)$ for different amplitude noise intensities V_N. Considering that the three cases of $V_c(\phi_N, V_N = 0)$ depend on f_{cp} (Fig. 1c), we examined $V_c(\phi_N)$ at $V_N > 0$ for $f_{cp} > f_{cp}^*$, $f_{cp} < f_{cp}^*$, and $f_{cp} \sim f_{cp}^*$, as shown in Fig. 2a–c, respectively. We also considered $V_c(\phi_N)$ at $V_N = 0$ for each case as a reference. As shown in Fig. 2a, $V_c(\phi_N)$, which shows a monotonic increase at $V_N = 0$, dramatically changes with increasing V_N and provides a nonmonotonic $V_c(\phi_N)$ for $V_N \geq 6$ V. However, for higher values of V_N (> 17 V), $V_c(\phi_N)$ exhibits a monotonic decrease. This result indicates that V_N can change the phase noise-induced monotonic increase in $V_c(\phi_N)$ into nonmonotonic behavior, indicating SR. Consequently, V_N can control $V_c(\phi_N)$ by using an appropriate combination of noises. In contrast, no remarkable change in $V_c(\phi_N)$ was observed at $f_{cp} < f_{cp}^*$ (Fig. 2b). Moreover, in the case of $f_{cp} \sim f_{cp}^*$ (Fig. 2c), the nonmonotonic $V_c(\phi_N)$ was maintained up to an appropriate intensity V_N but disappeared at higher V_N values (≥ 19 V). In Fig. 2, we used a colored amplitude noise with $f_{ca} < f_{ca}^*$ to obtain the abovementioned results. In addition, a different behavior of $V_c(\phi_N)$ was obtained when a colored amplitude noise with $f_{ca} > f_{ca}^*$ or $f_{ca} \sim f_{ca}^*$ was used (see below).

The amplitude noise-induced behavior of $V_c(V_N)$ for different phase intensities ϕ_N is shown in Fig. 3. This figure demonstrates more dramatic changes in $V_c(V_N)$, which indicate a transition between SR and ISR. In the case of $f_{ca} \sim f_{ca}^*$ and $f_{cp} \sim f_{cp}^*$ (Fig. 3a), an increase in ϕ_N induced smooth changes to the nonmonotonic $V_c(V_N)$, which indicates ISR for small ϕ_N values, to an almost constant $V_c(V_N)$ and then to a reversed nonmonotonic $V_c(V_N)$, indicating SR. Moreover, in the case of $f_{ca} \sim f_{ca}^*$ and $f_{cp} < f_{cp}^*$ (Fig. 3b), a similar change was observed; however, the detail of $V_c(V_N)$ was different in each case. For example, an intersection of $V_c(V_N)$ was found for $f_{cp} \sim f_{cp}^*$(Fig. 3a), indicating that a peculiar value of V_c could be determined by two ways using different ϕ_N (at a fixed V_N).

Finally, $V_c(\phi_N)$ and $V_c(V_N)$ in the f_{ca} and f_{cp} plane are shown in Fig. 4a, b, respectively. The case11 (C11) presented in Fig. 4a indicates the $V_c(\phi_N)$ shown in Fig. 2a, whereas C32 presented in Fig. 4b indicates the $V_c(V_N)$ shown in Fig. 3b. For $V_c(\phi_N)$, SR appears for wide regions of f_{cp} and f_{ca} by controlling V_N, except for $f_{cp} < f_{cp}^* - \Delta f_{cp}$. For $V_c(V_N)$, SR and ISR appear concurrently, and their transitions are indicated by the constant behavior symbol [although limited to narrow regions of f_{ca} (i.e., $f_{ca}^* - \Delta f_{ca} < f_{ca} < f_{ca}^* + \Delta f_{ca}$)]. In addition, an almost constant behavior of $V_c(V_N)$ was found during the transition between SR and ISR for $f_{ca}^* - \Delta f_{ca} < f_{ca} < f_{ca}^* + \Delta f_{ca}$ and during the change between monotonic increase and decrease for $f_{ca} > f_{ca}^* + \Delta f_{ca}$.

Experimental results for SR and ISR

In an electro-optical system for EC[35,36], we observed the emergence of SR and ISR by controlling both noises (i.e., ϕ_N and V_N) with appropriate f_{cp} and f_{ca} values. For reference, a conventional pattern evolution with increasing ϕ_N (at $V_N = 0$) was found at $V_0 = 18.8$ V [> $V_c(V_N = 0) = 17.8$ V], as shown in Fig. 5a [see the corresponding $V_c(\phi_N, V_N = 0)$ in Fig. 2a]. Since α decreased with increasing ϕ_N, the performance of EC patterns (or optical

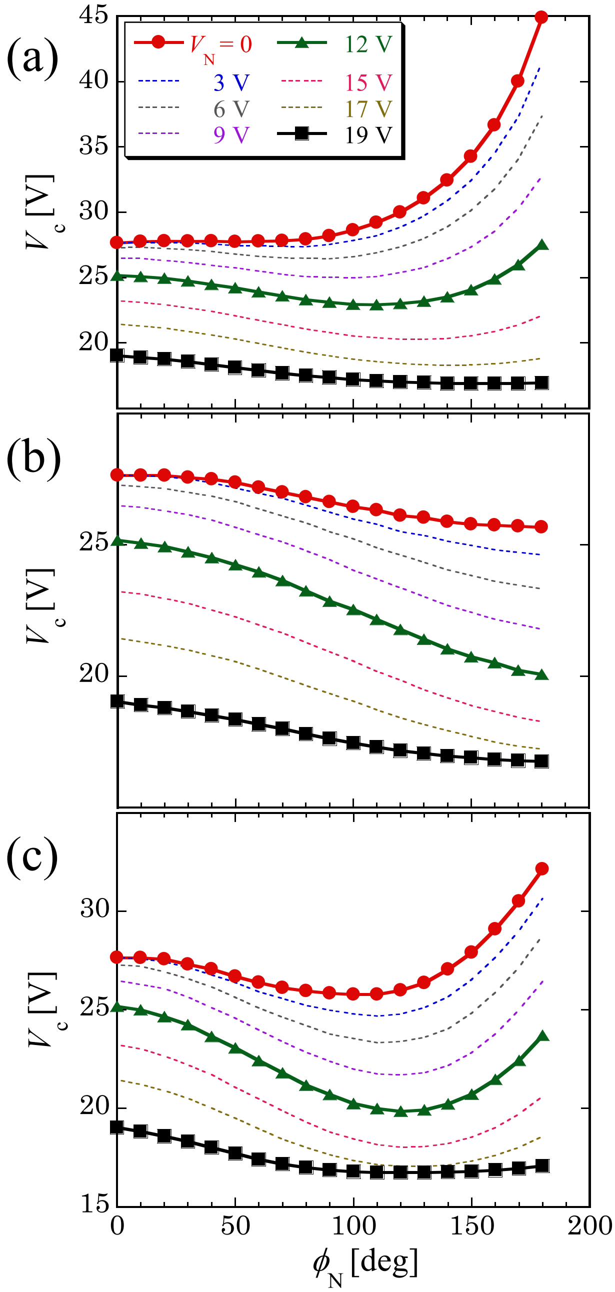

Figure 2. Behavior of $V_c(\phi_N)$ for various amplitude-noise intensities V_N with $f_{ca} < f_{ca}^*$. In the case of $f_0 = 2.5$ kHz and $f_{ca} = 100$ Hz ($< f_{ca}^* \approx 1$ kHz), V_c was determined using the phase noise with (**a**) $f_{cp} = 1$ kHz ($> f_{cp}^* \approx 100$ Hz), (**b**) $f_{cp} = 50$ Hz ($< f_{cp}^*$), and (**c**) $f_{cp} = 100$ Hz ($\approx f_{cp}^*$). A nonmonotonic $V_c(\phi_N)$ [e.g., at $V_N = 12$ V in (**a**,**c**)] indicates SR, as shown in Fig. 1c. When V_N is increased, a monotonic increase in $V_c(\phi_N)$ in (**a**) smoothly changes into a monotonic decrease through a nonmonotonic behavior. In contrast, the nonmonotonic behavior of $V_c(\phi_N)$ in (**c**) changes into a monotonic decrease for high V_N (≥ 19 V).

intensity $I \propto \varphi^2$)[40] decreased with increasing ϕ_N. Then, EC disappeared at $\phi_N = 40°$ for $\alpha < 0$ (i.e., $V_0 < V_c$). Such a pattern evolution is trivial and intuitive in the presence of conventional noise. Conversely, at $V_0 = 16.5$ V [$< V_c(V_N = 5$ V$) = 17.1$ V], SR was found, as shown in Fig. 5b [see the corresponding $V_c(\phi_N, V_N = 12$ V) in Fig. 2a]. By increasing ϕ_N, $\alpha < 0$ changed to $\alpha > 0$ and then again to $\alpha < 0$. Thus, EC smoothly appeared and disappeared with increasing ϕ_N. The EC performance (i.e., φ) showed a typical *bell-shaped* curve (i.e., SR), which is similar to the SR obtained from a single phase noise[25].

Figure 5c shows a unique pattern evolution with increasing V_N at $\phi_N = 90°$ and $V_0 = 18.3$ V [$> V_c(V_N = 0) = 17.8$ V]. A typical *reversed bell-shaped* curve of the EC performance indicating ISR was observed, which is similar to that of the ISR obtained from a single amplitude noise[17]. In addition, the present patterns at high V_N ($= 6-8$ V) showed localized ECs, which were not observed in a previous study based on a single amplitude

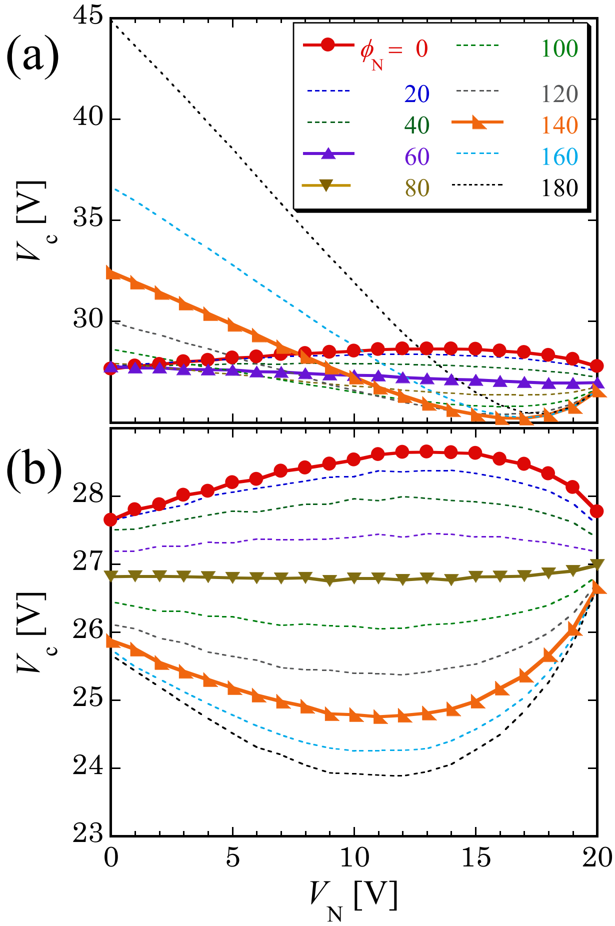

Figure 3. Behavior of $V_c(V_N)$ for various phase-noise intensities ϕ_N. In the case of $f_0 = 2.5$ kHz and $f_{ca} = 1$ kHz ($\approx f_{ca}^* \approx 1$ kHz), V_c was determined using the phase noise with (**a**) $f_{cp} = 100$ Hz ($\approx f_{cp}^*$) and (**b**) $f_{cp} = 50$ Hz ($< f_{cp}^*$). The nonmonotonic $V_c(V_N)$ [e.g., at $\phi_N = 140$ deg in (**a,b**)] indicates SR. Furthermore, the reversed nonmonotonic $V_c(V_N)$ [e.g., at $\phi_N = 0$ in (**a,b**)] indicates ISR, as shown in Fig. 1d. With an increase in the ϕ_N, the nonmonotonic behavior of $V_c(V_N)$ smoothly changes to reversed nonmonotonic behavior by exhibiting a nearly constant behavior [at $\phi_N = 60$ deg in (**a**) and $\phi_N = 80$ deg in (**b**)]; thus, a transition from ISR to SR is found by increasing ϕ_N.

noise[17]. Such localized patterns are attributed to the combined effect of both noises, indicating that comparatively high intensities of both noises may play a role in EC pattern structures as well as EC thresholds. In localized ECs that are stationary (not transient), a noise-induced abnormal distribution of electric charges for ECs may occur[41], which can be distinguished from the normal distribution of conventional ECs[34]. Such localized ECs are beyond the scope of our analysis using Eqs. (2) and (3). Evidently, our experimental observations revealed the crucial effects of colored amplitude and phase noises on the generation of both resonances through the smooth variation of the EC threshold. Unfortunately, the transition between SR and ISR (Fig. 3) was not observed due to experimental limitations, such as material parameters [e.g., τ, σ_H, λ, and η in Eqs. (2) and (3)] that are highly sensitive to V_c but difficult to tune to the values in the numerical study.

Discussion and conclusion

During the last four decades, SR has been intensively investigated in useful concepts of randomness[42] and extensively applied for noise benefits[42–44]. In this study, we presented an SR transitioned from ISR which has been less addressed so far in the literature. By examining the threshold of ac-driven EC, we showed that a suitable combination of colored amplitude and phase noises could induce the emergence of both resonances and the transition between them. Therefore, we demonstrated that SR and ISR, which have been independently reported so far, could be handled in a single framework. A recent numerical study on the co-occurrence of SR and ISR[16] reported in a neural system should be distinguished from this study. Such co-occurrence implies that an ISR exhibiting the minimal output for one performance measure (mean firing rate) can induce an SR exhibiting the maximal output for another performance measure (mutual information). Note that colored noise can vary the probability density of the state of systems, which is governed by the Fokker–Planck equation[45]. According to the correlation time of colored noise, the probability density distribution can also provide two peaks for two possible states ($\varphi = 0$ and $\varphi \neq 0$ in this study)[45].

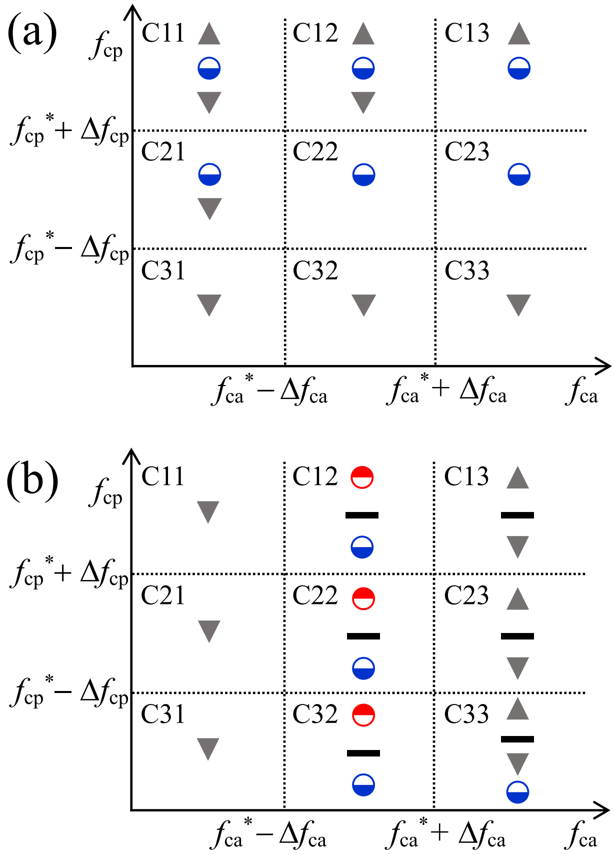

Figure 4. Phase diagrams of V_c in the f_{ca} and f_{cp} planes. (**a**) $V_c(\phi_N)$ for various V_N values. Notably, the symbols indicating $V_c(\phi_N)$ are arranged in the order in which V_N increases from top to bottom. Case11 (C11), C21 and C31 correspond to Fig. 2a, c, b, respectively. (**b**) $V_c(V_N)$ for various ϕ_N values. The symbols indicating $V_c(V_N)$ are arranged in the order in which ϕ_N increases from top to bottom. C12 and C32 correspond to Fig. 3a, b, respectively. The symbols filled triangle, downward filled triangle, and filled rectangle indicate monotonic increase, monotonic decrease, and constant behavior of V_c, respectively; blue circle filled at bottom and red circle filled at top indicate nonmonotonic and reversed nonmonotonic behavior of V_c, providing SR and ISR, respectively. In this numerical study, $f_0 = 2.5$ kHz, $f_{ca}^* \approx 1$ kHz, $f_{cp}^* \approx 100$ Hz, $\Delta f_{ca} \approx 500$ Hz, and $\Delta f_{cp} \approx 50$ Hz. See Supplementary Information for details.

In the Carr–Helfrich mechanism of ac-driven EC[32–36], the combined electric noises can play critical roles in the occurrence of EC through their effects on the motion of electric charges (by Coulomb force against the electro-elastic restoring force of the NLC) and vary the EC threshold. In particular, in the appropriate conditions of correlation times and intensities of the two noises, their roles can contradict each other, i.e., one may suppress EC and the other may promote EC. Consequently, this competition between the noise-induced stabilization and destabilization effects on EC is the underlying reason for the emergence of both resonances and their transition. If there exists a nonequilibrium, free energy-like potential[46] with its minima at $\varphi = 0$ and $\varphi \neq 0$ (i.e., a rest state and a convection state, respectively), which correspond to an ice state and a warm state, respectively, in the study of ice-age cycles[2,3], such a potential should be investigated along with its symmetry breaking[1,19] to understand the detail of the competition mechanism; and this is an important open question. Our numerical and experimental findings suggest that the control of SR and ISR by combining amplitude and phase noises can be very useful for electrical applications, such as sensing technologies[36,47,48] and brain science[12,13], for which additional phase noise can be readily introduced. Furthermore, the transition between SR and ISR may provide effective controls for desired and undesired performances in various related fields[49,50].

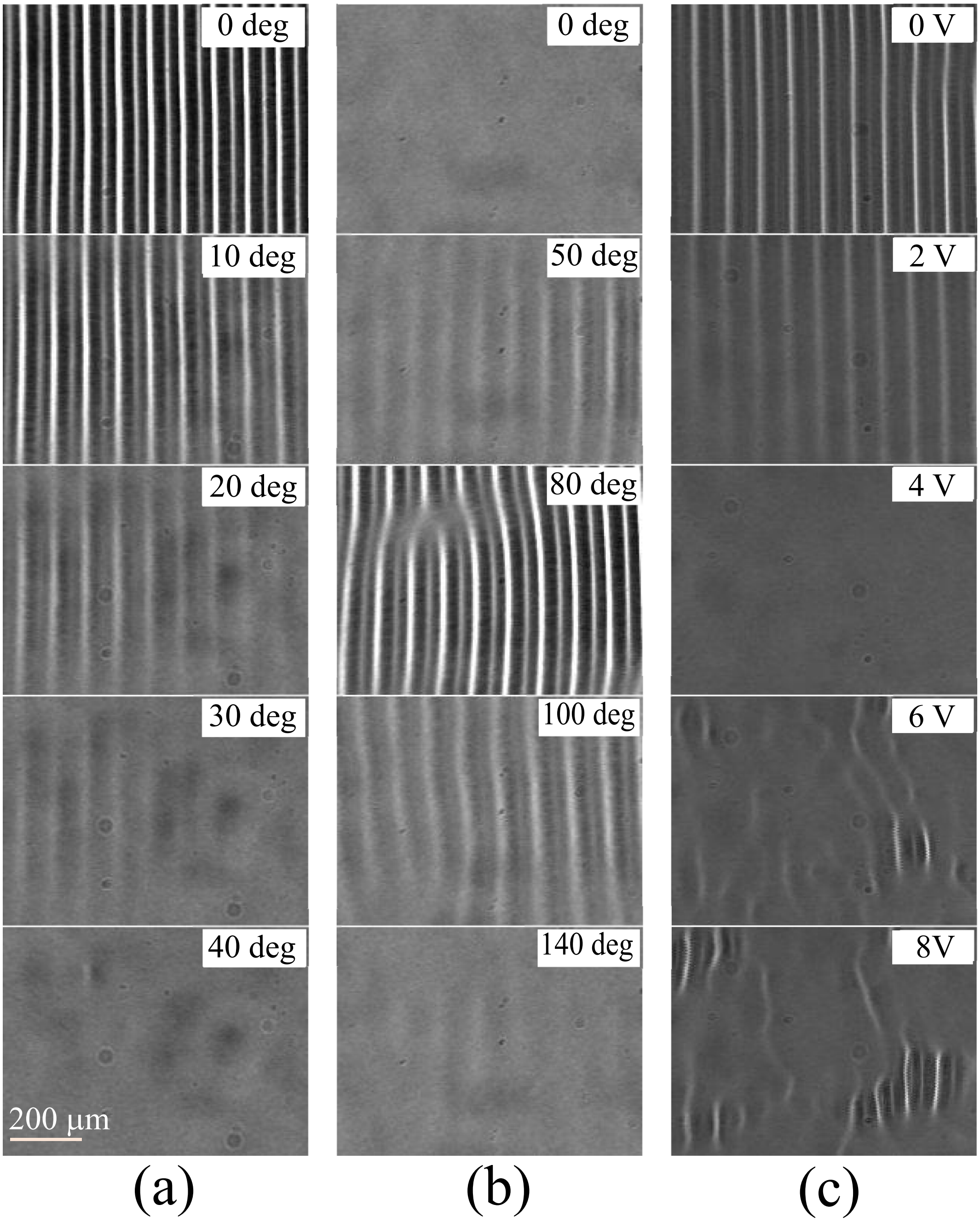

Figure 5. EC pattern evolutions with increasing ϕ_N or V_N. ECs were observed at $f_0 = 1.5$ kHz in a cell (MBBA, $d = 25$ μm). Phase noise ϕ_N with $f_{cp} = 2$ kHz smoothly increased when (**a**) $V_0 = 18.8$ V and $V_N = 0$ and (**b**) $V_0 = 16.5$ V and $V_N = 5$ V with $f_{ca} = 1$ kHz. (**c**) Amplitude noise V_N with $f_{ca} = 4.5$ kHz smoothly increased when $V_0 = 18.3$ V and $\phi_N = 90$ deg with $f_{cp} = 1.6$ kHz. Notably, (**a,b**) show pattern evolutions for $V_c(\phi_N)$ at $V_N = 0$ and $V_N = 12$ V in Fig. 2a, respectively, and (**c**) indicates that for $V_c(V_N)$ at $\phi_N = 20$ deg in Fig. 3b. SR and ISR are observed in (**b,c**), respectively. See Supplementary Information for details.

Data availability

The data that support the findings of this study are available from the corresponding author upon reasonable request.

Received: 30 May 2023; Accepted: 3 October 2023
Published online: 06 October 2023

References

1. Zhang, X.-J., Qian, H. & Qian, M. Stochastic theory of nonequilibrium steady states and its applications. Part I. *Phys. Rep.* **510**, 1 (2012).
2. Benzi, R., Sutera, A. & Vulpiani, A. The mechanism of stochastic resonance. *J. Phys. A* **14**, L453 (1981).
3. Benzi, R., Parisi, G., Sutera, A. & Vulpiani, A. Stochastic resonance in climate change. *Tellus* **34**, 10 (1982).
4. Dodda, A. *et al.* Stochastic resonance in MoS_2 photodetector. *Nat. Commun.* **11**, 4406 (2020).
5. Bhar, B., Khanna, A., Parihar, A., Datta, S. & Raychowdhury, A. Stochastic resonance in insulator–metal–transition systems. *Sci. Rep.* **10**, 5549 (2020).
6. Hohmann, W., Müller, J. & Schneider, F. W. Stochastic resonance in chemistry. *J. Phys. Chem.* **100**, 5388 (1996).
7. Suzuki, Y. & Asakawa, N. Stochastic resonance in organic electronic devices. *Polymers* **14**, 747 (2022).
8. Douglass, J. K., Wilkens, L., Pantazelou, E. & Moss, F. Noise enhancement of information transfer in crayfish mechanoreceptors by stochastic resonance. *Nature* **65**, 337 (1993).
9. Russell, D. F., Wilkens, L. A. & Moss, F. Use of behavioral stochastic resonance by paddle fish for feeding. *Nature* **402**, 291 (1999).
10. Simonotto, E. *et al.* Visual perception of stochastic resonance. *Phys. Rev. Lett.* **78**, 1186 (1997).
11. Roy, P. K. & Rallabandi, V. P. S. Magnetic resonance imaging (MRI) enhancement using stochastic resonance. *Magn. Reson. Imaging* **28**, 1361 (2010).
12. Gluckman, B. J. *et al.* Stochastic resonance in a neuronal network from the mammalian brain. *Phys. Rev. Lett.* **77**, 4098 (1996).
13. Kai, S. & Mori, T. Noise-induced entrainment and stochastic resonance in human brain waves. *Phys. Rev. Lett.* **88**, 218101 (2002).
14. Gutkin, B., Jost, J. & Tuckwell, H. C. Inhibition of rhythmic neural spiking by noise: the occurrence of a minimum in activity with increasing noise. *Naturwissenschaften* **96**, 1091 (2009).
15. Uzuntarla, M., Cressman, J. R., Ozer, M. & Barreto, E. Dynamical structure underlying inverse stochastic resonance and its implications. *Phys. Rev. E* **88**, 042712 (2013).
16. Zamani, A., Novikov, N. & Gutkin, B. Concomitance of inverse stochastic resonance and stochastic resonance in a minimal bistable spiking neural circuit. *Commun. Nonlinear Sci. Numer. Simulat.* **82**, 105024 (2020).
17. Huh, J.-H. Inverse stochastic resonance in electroconvection by multiplicative colored noise. *Phys. Rev. E* **94**, 052702 (2016).
18. Touboul, J. D., Staver, A. C. & Levin, S. A. On the complex dynamics of savanna landscapes. *Proc. Natl. Acad. Sci. USA* **115**, E1336 (2018).
19. Torres, J. J., Uzuntarla, M. & Marro, J. A theoretical description of inverse stochastic resonance in nature. *Commun. Nonlinear Sci.* **80**, 104975 (2020).
20. Sutera, A. On stochastic perturbation and long-term climate behavior. *Q. J. R. Meteorol. Soc.* **107**, 137 (1981).
21. Nicolis, G. & Altares, V. A new method of analysis of the effect of weak colored noise in nonlinear dynamical systems. *J. Stat. Phys.* **46**, 191 (1987).
22. Jia, Y., Zheng, X., Hu, X. & Li, J. Effects of colored noise on stochastic resonance in a bistable system subject to multiplicative and additive noise. *Phys. Rev. E* **63**, 031107 (2001).
23. Gammaitoni, L., Marchesoni, F., Menichella-Saetta, E. & Santucci, S. Multiplicative stochastic resonance. *Phys. Rev. E* **49**, 4878 (1994).
24. Seki, K. & Barzykin, A. V. Stochastic resonance driven by Gaussian multiplicative noise. *Europhys. Lett.* **40**, 117 (1997).
25. Huh, J.-H., Yano, Y. & Miyagawa, N. Phase noise can induce stochastic resonance?. *J. Phys. Soc. Jpn.* **88**, 063001 (2019).
26. Chowdhury, A., Barbay, S., Clerc, M. G., Robert-Philip, I. & Braive, R. Phase stochastic resonance in a forced nanoelectromechanical membrane. *Phys. Rev. Lett.* **119**, 234101 (2017).
27. Huh, J.-H. Noise-induced threshold shift and pattern formation in electroconvection by controlling characteristic time scales. *Phys. Rev. E* **84**, 025302(R) (2011).
28. Huh, J.-H. & Kai, S. Colored noise-induced threshold shifts and phase diagrams in electroconvections. *J. Phys. Soc. Jpn.* **83**, 063601 (2014).
29. Y. Yamamoto and D. Nozaki, Enhancement of stochastic resonance in a FitzHugh-Nagumo neuronal model driven by colored noise, Phys. Lett., A **243**, 281(1998).
30. Nozaki, D., Mar, D. J., Grigg, P. & Collins, J. J. Effects of colored noise on stochastic resonance in sensory neurons. *Phys. Rev. Lett.* **82**, 2402 (1999).
31. Guo, D. Inhibition of rhythmic spiking by colored noise in neural systems. *Cogn. Neurodyn.* **5**, 293 (2011).
32. Carr, E. F. Influence of electric fields on the molecular alignment in the liquid crystal *p*-(anisalamino)-phenyl acetate. *Mol. Cryst. Liq. Cryst.* **7**, 253 (1969).
33. Helfrich, W. Conduction-induced alignment of nematic liquid crystals: Basic model and stability considerations. *J. Chem. Phys.* **51**, 4092 (1969).
34. Smith, I. W., Galerne, Y., Lagerwall, S. T., Dubois-Violette, E. & Durand, G. Dynamics of electrohydrodynamic instabilities in nematic liquid crystals. *J. Phys (Paris)* **36**, C1-237 (1975).
35. Prost, J. & de Gennes, P. G. *The Physics of Liquid Crystals* (Claerendon, 1993).
36. Eber, N., Salamon, P. & Buka, A. Electrically induced patterns in nematics and how to avoid them. *Liq. Cryst. Rev.* **4**, 101 (2016).
37. Kawakubo, T., Yanagita, A. & Kabashima, S. External noise effect on the onset of Williams domain in nematic liquid crystals. *J. Phys. Soc. Jpn.* **50**, 1451 (1981).
38. Huh, J.-H. Multiplicative noise effects on electroconvection in controlling additive noise by a magnetic field. *Phys. Rev. E* **92**, 062504 (2015).
39. Kai, S., Kai, T., Takata, M. & Hirakawa, K. Effect of the white noise on electrohydrodynamic transitions in nematics. *J. Phys. Soc. Jpn.* **47**, 1379 (1979).
40. John, T. & Stannarius, R. Preparation of subharmonic patterns in nematic electroconvection. *Phys. Rev. E* **70**, 025202(R) (2004).
41. Huh, J.-H. Traveling waves and worms in ac-driven electroconvection under external multiplicative noise. *Phys. Rev. E* **95**, 042704 (2017).
42. McDonnell, M. D. & Abbott, D. What is stochastic resonance? Definitions, misconceptions, debates, and its relevance to biology. *PLoS Comput. Biol.* **5**, e1000348 (2009).
43. Gammaitoni, L., Hänggi, P., Jung, P. & Marchesoni, F. Stochastic resonance. *Rev. Mod. Phys.* **70**, 223 (1998).
44. Budrikis, Z. Forty years of stochastic resonance. *Nat. Rev. Phys.* **3**, 771 (2021).
45. Sancho, J. M. & Miguel, M. S. Langevin equations with colored noise. In *Noise in Nonlinear Dynamics Systems*. Vol. 1. *Theory of Continuous Fokker–Planck Systems* (Eds. Moss, F., McClintock, P. V. E.) (Cambridge University Press, 1989) (Lugiato, L. A., Broggi, G., Merri, M. & Pernigo, M. A. Control of noise and applications to optical systems. Ibid. Vol. 2. *Theory of Noise-Induced Processes in Special Applications*).
46. Wio, H. S. *et al.* The nonequilibrium potential today: A short review. *Chaos Solit. Fract.* **165**, 112778 (2022).
47. Collins, J. J., Imhoff, T. T. & Grigg, P. Noise-mediated enhancements and decrements in human tactile sensation. *Phys. Rev. E* **56**, 923 (1997).
48. Dong, H. *et al.* Adaptive intrawell matched stochastic resonance with a potential constraint-aided line enhancer for passive sonars. *Sensors* **20**, 3269 (2020).
49. Horsthemke, W. & Lefever, R. *Noise-Induced Transitions* (Springer, 1984).

50. Ridolfi, L., D'Odorico, P. & Laio, F. *Noise-Induced Phenomena in Environmental Sciences* (Cambridge University Press, 2011).

Acknowledgements
This work was supported by JSPS KAKENHI Grant Number 22K03470.

Author contributions
J.-H.H. conceived the research. N.M. and M.S. performed the numerical analysis. J.-H.H. and M.S. carried out the experimental examination. All authors contributed to all aspects of this work.

Competing interests
The authors declare no competing interests.

Additional information
Supplementary Information The online version contains supplementary material available at https://doi.org/10.1038/s41598-023-44043-4.

Correspondence and requests for materials should be addressed to J.-H.H.

Reprints and permissions information is available at www.nature.com/reprints.

Publisher's note Springer Nature remains neutral with regard to jurisdictional claims in published maps and institutional affiliations.

Scientific Reports Supplementary Information

Control of stochastic and inverse stochastic resonances in a liquid-crystal electroconvection system using amplitude and phase noises

Jong-Hoon Huh*, Masato Shiomi, and Naoto Miyagawa

Department of Physics and Information Technology, Faculty of Computer Science and Systems Engineering, Kyushu Institute of Technology, Fukuoka 820-8502, Japan

*Corresponding author: huh@phys.kyutech.ac.jp

Supplementary Methods

Numerical calculation. We used the discrete fourth-order Runge-Kutta method in a versatile software package (MATLAB R2020b) to determine the threshold voltage V_c of electroconvection (EC) from the governing Carr-Helfrich Eqs. (2) and (3). V_c can be determined as the lowest value V in the numerical loop with an increment of $\Delta V = 0.1$ V for which the director angle φ does not relax to zero [34]. The colored noise, with a cutoff frequency f_{ca} for amplitude noise or f_{cp} for phase noise, was provided by a built-in frequency filtering program within the software. The parameters for the nematic liquid crystal (NLC) [i.e., *p*-methoxybenzylidene-*p*'-*n*-butylaniline (MBBA)] and the control parameters are shown in Table 1 [34,35].

Table 1. Material and control parameters used in this study.

material parameters (SI units) *1)			control parameters		
calculation		experiment	calculation		experiment
$\varepsilon_{//}$	4.605		f_0	2.5 kHz	1.5 kHz
$\varepsilon_{\perp}$	5.032	5.16	V_0	10–50 V	10–20V
$\sigma_{//}$	6.14×10^{-8}		f_{cp}	0.05–5 kHz	1.6 kHz
$\sigma_{\perp}$	5.13×10^{-8}	1.13×10^{-8}	f_{ca}	0.05–2 kHz	4.5 kHz
γ_1	0.0755				
γ_2	−0.0785		ϕ_N	0–180 deg	0–180 deg
α_v	0.1986				
K_{33}	6.53×10^{-12}		V_N	0–20 V	0–10 V
k	1.26×10^{5}				

*1) see Refs. 34 and 35 for the details of parameters for Eqs. (2) and (3): conductivity anisotropy $\sigma_a = \sigma_{//} - \sigma_{\perp}$, dielectric anisotropy $\varepsilon_a = \varepsilon_{//} - \varepsilon_{\perp}$, charge relaxation time $\tau = (\varepsilon_0\varepsilon_{//})/\sigma_{//}$, director relaxation constant λ, Helfrich parameter σ_H, equivalent field E_0 including elastic constant K_{33} and wavenumber k of EC, and effective viscosity η determined by real viscosity constants γ_1, γ_2 and α_v: $\sigma_H = \sigma_{//}\left(\frac{\varepsilon_{\perp}}{\varepsilon_{//}} - \frac{\sigma_{\perp}}{\sigma_{//}}\right)$, $\lambda = \varepsilon_0 |\varepsilon_a| \frac{\varepsilon_{\perp}}{\varepsilon_{//}}\left(\frac{1}{\gamma_1} + \frac{1}{\eta_0}\right)$, $E_0^2 = \frac{\varepsilon_{//}}{\varepsilon_0|\varepsilon_a|\varepsilon_{\perp}} K_{33}k^2$,

$\frac{1}{\eta} = \frac{1}{\eta_0}\left(\frac{2\gamma_1}{\gamma_1 - \gamma_2}\right) + \frac{|\varepsilon_a|}{\varepsilon_{//}}\left(\frac{1}{\gamma_1} + \frac{1}{\eta_0}\right)$, $\eta_0 = \left(\frac{\gamma_1}{\alpha_2}\right)^2\left(\frac{1}{2}\alpha_v - \frac{\alpha_2^2}{\gamma_1}\right)$, $a_2 = \frac{1}{2}(\gamma_2 - \gamma_1)$.

In general, the threshold voltage V_c can be calculated in the pure ac field with a frequency f_0 by the following equation:

$$V_c^2(f_0) = V_0^2(1 + 4\pi^2 f_0^2\tau^2)/[\delta^2 - (1 + 4\pi^2 f_0^2\tau^2)].$$

Here, τ and δ^2 correspond to the charge relaxation time and the Helfrich parameter, respectively [34,35]. In the presence of noise [Eq. (4)], the variation of V_c was numerically determined as a function of the amplitude noise intensity V_N and the phase noise intensity ϕ_N.

Experimental procedure. A typical NLC (i.e., MBBA) [34,35] was injected into a planar alignment cell with two parallel transparent indium tin oxide electrodes (E.H.C., Ltd, Japan). In this cell, the director $\boldsymbol{n}$ ($|\boldsymbol{n}| = 1$, $\boldsymbol{n} \equiv -\boldsymbol{n}$), which indicates a locally averaged direction of rod-like molecules in the NLC, homogenously tends to the preferred direction (the $\boldsymbol{x}$ axis in this study) before EC (i.e., for $V < V_c$). The application of an initial voltage $V_0(t)[= E(t)d = \sqrt{2}V_0 \cos 2\pi f_0 t]$ across the thin NLC layer with a thickness d (d = 25 μm in this study) [$\boldsymbol{E}(t)$ // $\hat{z}$] electrohydrodynamically destabilizes the anisotropic fluid (i.e., NLC) by the Carr-Helfrich mechanism [32-36]. The EC was observed at V_c by the lens effect of the periodic director modulation [35,36]. The function $V_c(f_0)$ was experimentally confirmed in one- [51,52] and two- [35,36,53] dimensional cells. To generate colored amplitude and phase noises, two noise generators (HSA4051, NF) were used, which could control the cutoff frequencies f_{ca} and f_{cp} through low pass filters [54,55]. The filters allow low-frequency components to pass through but attenuate components with frequencies higher than f_{ca} and f_{cp}. The noise generated by NG-2 was introduced into the original wave generator SWG (WF1974, NF), which played a role as phase noise; the amplitude noise was generated by NG-1and combined through a combiner (50PD-016, JFW) with the voltage modulated by phase noise, as shown in Fig. 1e. The optical patterns for EC were observed in the *xy* plane using computer-controlled image software (Scion Image) and an image-capture board (PCI-VE5, Scion Corp.) together with a charge-coupled device camera (XC-75, Sony) mounted on a polarizing microscope (ML9300, Olympus). The experiment was carried out at a stable temperature (T = 25 ± 0.2 °C) using a temperature controller (TH-99, Japan Hightech).

References

51. J. -H. Huh and S. Kai, Electroconvection in nematic liquid crystals in Hele-Shaw cells, Phys. Rev. E **68**, 042702 (2003).
52. J. -H. Huh, Electroconvection in one-dimensional liquid crystal cells, Phys. Rev. E **97**, 042707 (2018).
53. K. Hirakawa and S. Kai, Analogy between hydrodynamic instabilities in nematic liquid crystal and classical fluid, Mol. Cryst. Liq. Cryst. **40**, 261 (1977).
54. J. -H. Huh, Influence of external noise on various electrohydrodynamic instabilities in a nematic liquid crystal, J. Phys. Soc. Jpn. **81**, 104602 (2012).
55. O. J. Ushie, M. Abbod, E. C. Ashigwuike, and S. Lawan, Constrained nonlinear optimization of unity gain operational amplifier filters using PSO, GA and Nelder-Mead, Inter. J. Intelligent Control and Systems, **20**, 26 (2015).

Supplementary Results

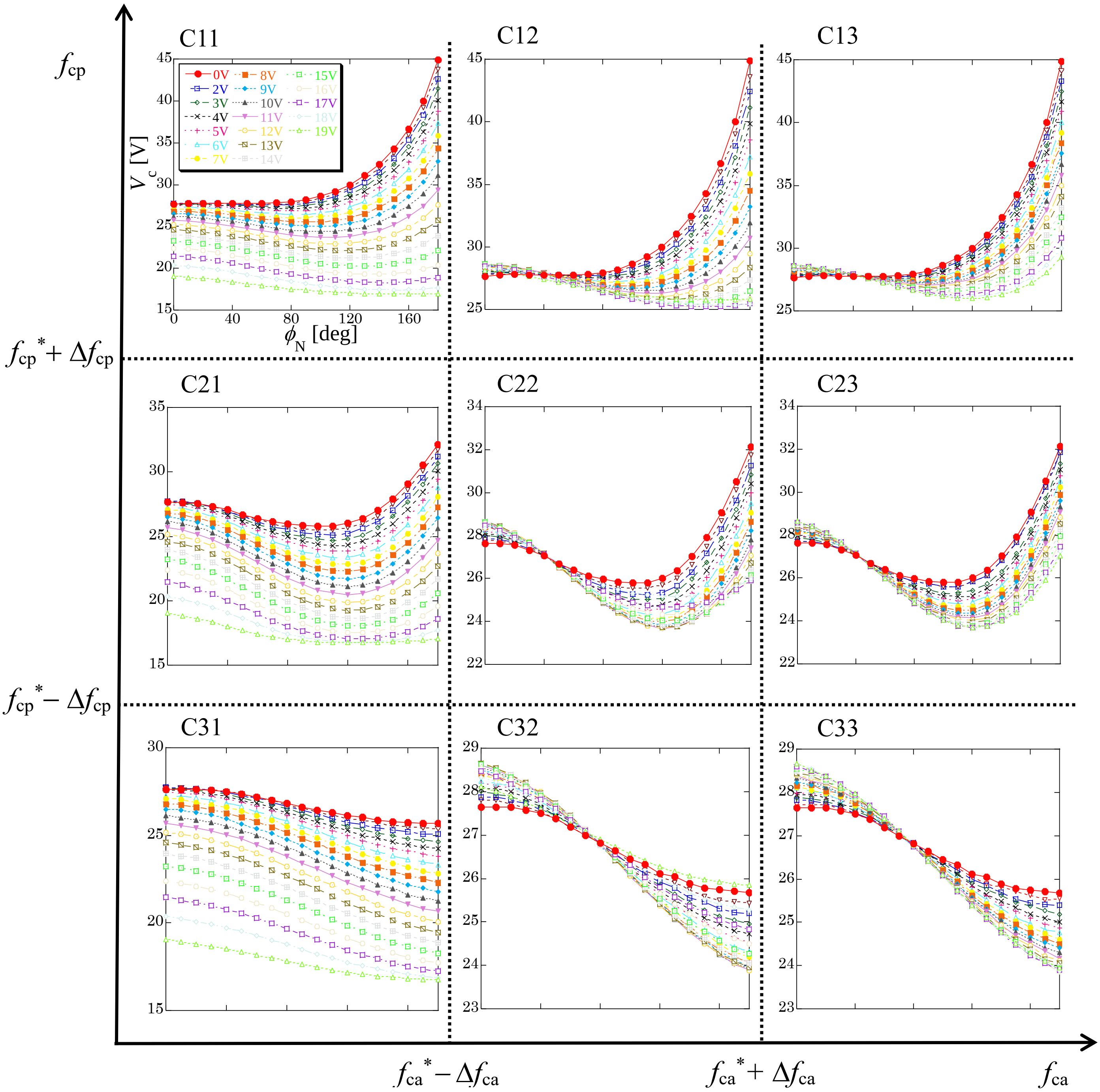

Supplementary FIG. (a) The threshold function $V_c(\phi_N)$ for various V_N values in the f_{ca} and f_{cp} plane. This corresponds to Fig. 4a.

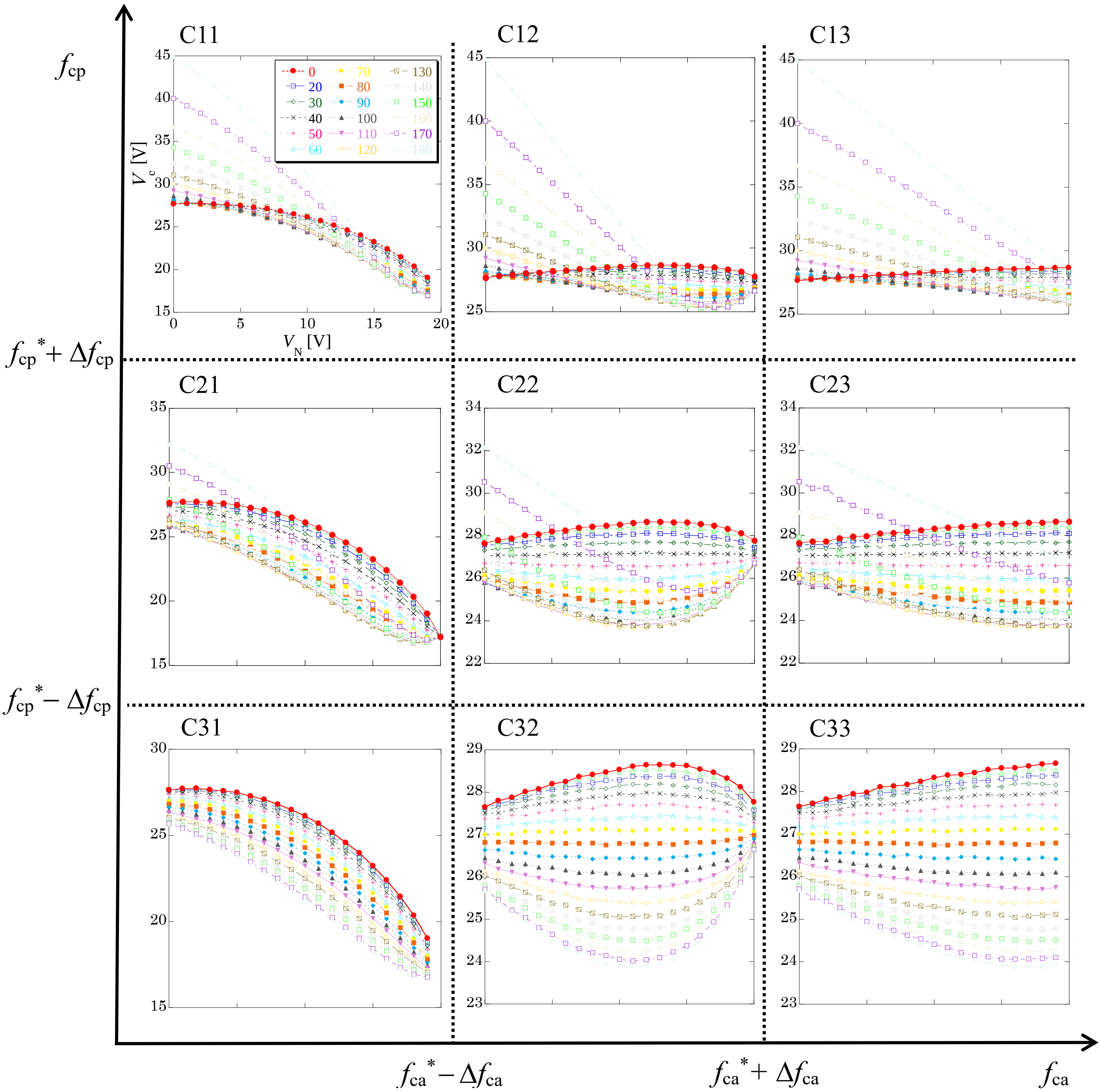

Supplementary FIG. (b) The threshold function $V_c(V_N)$ for various ϕ_N values in the f_{ca} and f_{cp} plane. This corresponds to Fig. 4b.